Hindawi Publishing Corporation
Advances in Acoustics and Vibration
Volume 2016, Article ID 7428616, 13 pages
http://dx.doi.org/10.1155/2016/7428616

Research Article

Mixed Skyhook and FxLMS Control of a Half-Car Model with Magnetorheological Dampers

Piotr Krauze and Jerzy Kasprzyk

Institute of Automatic Control, Silesian University of Technology, Akademicka 16, Gliwice, Poland

Correspondence should be addressed to Piotr Krauze; piotr.krauze@polsl.pl

Received 30 July 2016; Accepted 5 October 2016

Academic Editor: Mohammad Tawfik

The problem of vibration attenuation in a semiactive vehicle suspension is considered. The proposed solution is based on usage of the information about the road roughness coming from the sensor installed on the front axle of the vehicle. It does not need any preview sensor to measure the road roughness as other preview control strategies do. Here, the well-known Skyhook algorithm is used for control of the front magnetorheological (MR) damper. This algorithm is tuned to a quarter-car model of the front part of the vehicle. The rear MR damper is controlled by the FxLMS (Filtered-x LMS) taking advantage of the information about the motion of the front vehicle axle. The goal of this algorithm is to minimize pitch of the vehicle body. The strategy is applied for a four-degree-of-freedom (4-DOF) vehicle model equipped with magnetorheological dampers which were described using the Bouc-Wen model. The suspension model was subjected to the road-induced excitation in the form of a series of bumps within the frequency range 1.0–10 Hz. Different solutions are compared based on the transmissibility function and simulation results show the usefulness of the proposed solution.

1. Introduction

Damping of mechanical vibrations in vehicles using passive solution has a very long history and is widely used in practice. The conventional passive suspension system consists of a combination of springs and dampers. The characteristics of such suspension elements cannot be altered during operation. In recent years, much research has been carried out in the design of active and semiactive suspensions of vehicles for control of vibrations. However, active vibration damping entails considerable cost and difficulty in implementation of systems of this type; thus in the second half of the twentieth century a compromise between passive and active systems has been proposed. The semiactive suspension is an alternate to the active suspension [1]. Between different semiactive devices, magnetorheological (MR) dampers have received considerable interest in the last two decades [2]. These dampers comprise MR fluid belonging to the class of smart materials. The essential feature of MR fluid is its ability to reversibly change the state from a viscous to a semisolid with controllable yield strength when it is subjected to an external magnetic field. Varying electric current flowing through coils mounted in the piston of the damper allows for changing dynamical properties of the MR fluid. Inherent stability and low power consumption is favoured over active suspension force generators, so MR dampers are widely used in vehicle suspension systems [3–5].

Skyhook algorithm is one of the most widely used feedback control schemes dedicated to semiactive dampers firstly proposed in [1] and analysed based on a quarter-car model. The Skyhook control is favoured for its robustness and low complexity which is especially important in case of real-time applications, for example, [3]. Numerous scenarios of Skyhook control were already published including control of quarter-car model [6] or plants modelled as quarter-car, for example, passenger's seat [7] or bicycle [8]. The classical Skyhook algorithm can be also used for separate control of each vehicle suspension part of a half-car experimental model [9] or a real-size vehicle [4]. Other variants of Skyhook control are related to coupled control of vehicle body vibration

modes, that is, heave, pitch, and roll modes [10], or Skyhook control accompanied with procedure of its parameters adaptation [11].

The performance of the semiactive suspension system can be improved by knowing the future information about the road input, which is referred to as *preview control*. The semiactive suspension system with preview control using the linear quadratic theory was applied to quarter-car [12] and half-car [13] vehicle models. Stochastic optimal preview control of a vehicle suspension was presented in [14] and control using the H_∞ theory in [15]. The other approach, based on the FxLMS algorithm modified for semiactive devices, was tested in [16] for a quarter-car model and in [17] for a half-car model. In all these references it is assumed that some kind of information about the road roughness is available in advance. However, in practice, the problem of the appropriate measurement of the road profile that can be available and useful for the control algorithm in real-time is very difficult. It can be obtained using specialized vision systems or laser scanners aimed in front of the vehicle. These devices are expensive and measurements are subjected to different disturbances or distortions; for example, quality of the information depends on lighting conditions [18]. Thus, they require sophisticated algorithms of measurement data processing [19]. In [20] it was proposed to use the lead vehicle response to generate preview functions for active suspension of convoy vehicles, but, of course, it is not the solution for normal civil vehicles. In this paper it is proposed to improve the quality of vibration control in a semiactive suspension by *adaptive semipreview* control. In this approach it is assumed that the front part of the suspension will be controlled without any information about the road, for example, using the Skyhook algorithm [1], whereas adaptive control of the rear part of the suspension can take advantage of the road roughness obtained due to the information about the movement of the front part. We proposed to use the FxLMS algorithm to control pitch of the vehicle body.

The paper is organized as follows. Section 2 refers to an experimental setup and defines a half-car model used in the research. In Section 2.2 behaviour of the MR damper is analysed and the required models of dynamics are obtained. Section 3 introduces the proposed semiactive vibration control algorithm. In Section 4 simulation results are presented and discussed as well as concluded in Section 5.

2. Modelling of Experimental Setup

Presented studies are related to the model of the experimental all-terrain vehicle equipped with magnetorheological dampers and vibration control system [21]. The vehicle is 2 meters long and 1 meter wide and it weighs 340 kilograms. The original shock absorbers in the vehicle were replaced with the suspension MR dampers produced by Lord Corporation. The measurement part of the system consists of numerous sensors, such as accelerometers, gyroscopes, and vehicle speed sensors, which track the vehicle motion during its ride. The motion of the vehicle body and underbody parts is measured using eight 3-axis accelerometers located in the vehicle

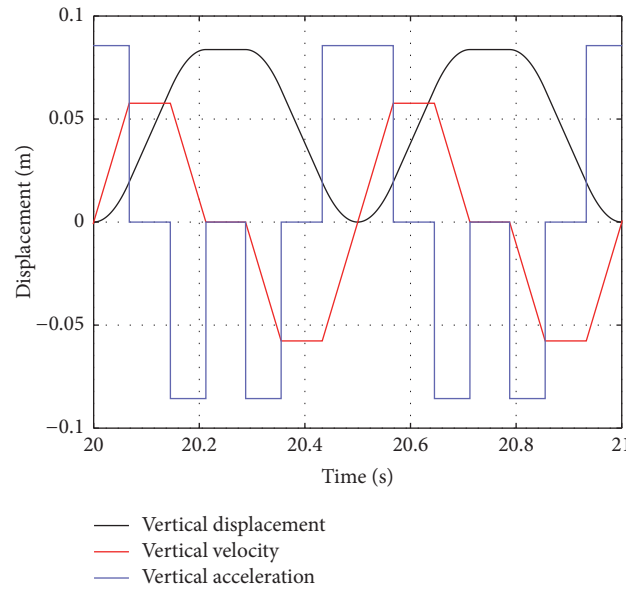

Figure 1: Simulated series of road bumps.

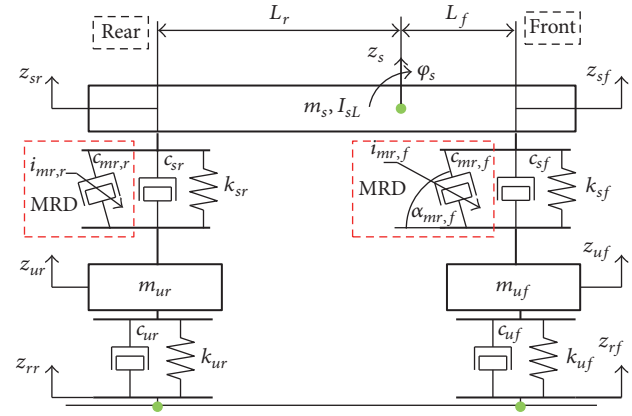

Figure 2: Half-car model of vehicle dynamics.

body as well as installed near the vehicle wheels. The vehicle speed is validated using the Hall effect sensors installed near the wheels. Moreover, vehicle suspension deflection sensors and inertial measurement units are applied.

2.1. Half-Car Model of Vehicle Dynamics. Generally, a full-car vehicle model which exhibits seven degrees of freedom [22] is used for the vibration control analysis. Such model maps heave, pitch, and roll motion of the vehicle body part as well as vertical motion of each wheel. The vehicle under consideration can be assumed with a high accuracy as longitudinally symmetrical. Vibrations of the right and left part of the vehicle are symmetrically excited using the simulated road-induced excitation, composed of a series of road bumps (see Figure 1). Therefore, a roll angle motion can be safely neglected in the analysis and it is sufficient to consider only a half-car model with 4 DOFs (see Figure 2).

In the particular case vibrations of the vehicle body part could be ideally decoupled which means that road

excitation of the front vehicle part induces vibration of only front vehicle part and similarly for the rear vehicle part. Thus, double quarter-car models were also considered for simulation studies. However, generally, such assumption is not valid for the real vehicles. Furthermore, in the case of the experimental vehicle to which the presented studies are dedicated, vibration coupling between the front and the rear vehicle parts can be clearly measured. Thus, the following analysis is limited to the heave and pitch of the vehicle body as well as to the vertical motion of the wheels.

Dynamics of the road vehicle can be modelled by the following differential equations:

$$\begin{aligned}
m_s\ddot{z}_s &= -k_{sf}\left(z_{sf}-z_{uf}\right)-c_{sf}\left(\dot{z}_{sf}-\dot{z}_{uf}\right)+F_{mr,f}\\
&\quad\cdot\sin\left(\alpha_{mr,f}\right)-k_{sr}\left(z_{sr}-z_{ur}\right)-c_{sr}\left(\dot{z}_{sr}-\dot{z}_{ur}\right)\\
&\quad+F_{mr,r}\sin\left(\alpha_{mr,r}\right),\\
I_{sL}\ddot{\varphi}_s &= L_f\left[k_{sf}\left(z_{sf}-z_{uf}\right)+c_{sf}\left(\dot{z}_{sf}-\dot{z}_{uf}\right)\right.\\
&\quad\left.-F_{mr,f}\sin\left(\alpha_{mr,f}\right)\right]-L_r\left[k_{sr}\left(z_{sr}-z_{ur}\right)\right.\\
&\quad\left.+c_{sr}\left(\dot{z}_{sr}-\dot{z}_{ur}\right)-F_{mr,r}\sin\left(\alpha_{mr,r}\right)\right],\\
m_{uf}\ddot{z}_{uf} &= -k_{uf}\left(z_{uf}-z_f\right)-c_{uf}\left(\dot{z}_{uf}-\dot{z}_f\right)-F_{mr,f}\\
&\quad\cdot\sin\left(\alpha_{mr,f}\right)+k_{sf}\left(z_{sf}-z_{uf}\right)+c_{sf}\left(\dot{z}_{sf}-\dot{z}_{uf}\right),\\
m_{ur}\ddot{z}_{ur} &= -k_{ur}\left(z_{ur}-z_r\right)-c_{ur}\left(\dot{z}_{ur}-\dot{z}_r\right)-F_{mr,r}\\
&\quad\cdot\sin\left(\alpha_{mr,r}\right)+k_{sr}\left(z_{sr}-z_{ur}\right)+c_{sr}\left(\dot{z}_{sr}-\dot{z}_{ur}\right),
\end{aligned}\tag{1}$$

where subscripts f and r denote the front and rear part of the suspension, respectively. The sprung and unsprung parts of the vehicle are denoted using subscripts s and u, respectively. In the further analysis linear and angular velocities will be denoted as v and ω, respectively; namely, $v_s = \dot{z}_s$ and $\omega_s = \dot{\varphi}_s$. The linear and angular accelerations will be denoted as a and ε, respectively; namely $a_s = \ddot{z}_s$ and $\varepsilon_s = \ddot{\varphi}_s$. Location of the vehicle body's centre of gravity is described by distances L_f and L_r. Vertical displacements of the vehicle body z_{sf} and z_{sr} can be defined as

$$\begin{aligned}
z_{sf} &= z_s - L_f\varphi_s,\\
z_{sr} &= z_s + L_r\varphi_s.
\end{aligned}\tag{2}$$

The road-induced displacements exciting the front and rear part of the vehicle are denoted as z_{rf} and z_{rr}. Vibrations propagate into the unsprung and sprung parts resulting in vertical displacement of wheels denoted as z_{uf} and z_{ur} and vertical displacement of the front and rear vehicle body as z_{sf} and z_{sr}, respectively. Parameters of the half-car model are listed as below.

Parameters of the Simulated 4 DOFs Half-Car Model

$L_f = 1.116\,\text{m}$,
$L_r = 1.232\,\text{m}$,
$m_s = 348\,\text{kg}$,
$I_{sL} = 175.2\,\text{kgm}^2$,
$k_{sf} = 28.0\,\text{kNm}^{-1}$,
$k_{sr} = 30.4\,\text{kNm}^{-1}$,
$c_{sf} = 971\,\text{Nsm}^{-1}$,
$c_{sr} = 2464\,\text{Nsm}^{-1}$,
$m_{uf} = 23.7\,\text{kg}$,
$m_{ur} = 64.3\,\text{kg}$,
$k_{uf/ur} = 169\,\text{kNm}^{-1}$,
$c_{uf/ur} = 883\,\text{Nsm}^{-1}$,
$\alpha_{mr,f} = 63^\circ$,
$\alpha_{mr,r} = 63^\circ$.

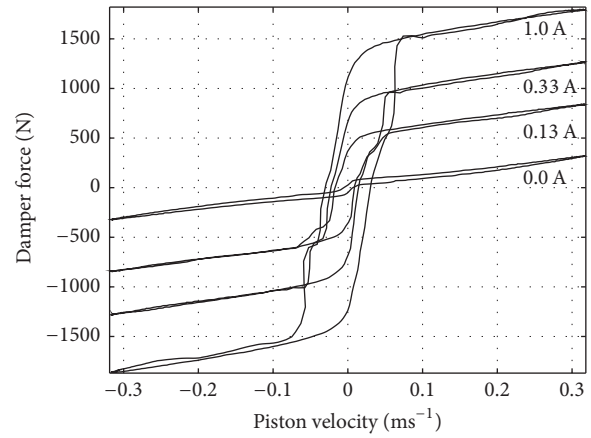

Figure 3: MR damper velocity-force characteristics.

The response of the vehicle to the bump excitation is mainly influenced by stiffness and viscous damping of the vehicle tires and the suspension system, denoted here by k and c. Stiffness of the tire corresponds to the pressure of compressed air therein. Passive invariant stiffness of the vehicle suspension describes behaviour of the shock absorbers. Viscous damping of the suspension is mainly related to passive damping of the shock absorbers, but it also corresponds to the overall and distributed suspension damping.

2.2. MR Damper Model. Axial force generated by the MR damper can change from hundreds to thousands of newtons in a couple of milliseconds [23]. However, due to the complex composition of the MR fluid inside the damper, this device exhibits strongly nonlinear behaviour. The velocity-force characteristics reveal saturation regions and hysteretic loop [3]. An exemplary characteristic for different current levels obtained for the MR damper produced by Lord Corporation is presented in Figure 3.

Numerous models are known in the literature that deal with these phenomena [24]. The Bingham model [25] includes viscous damping and Coulomb friction components. Extension of the Bingham model which additionally

applies Kelvin-Voight body and Hooke body models is known as Gamota-Filisko model [2]. An accurate MR damper model needs to take into account numerous dependencies of the resultant force on control current, excitation magnitude, and frequency which was extensively reviewed in [26]. The proposed model was additionally validated and applied in control [27].

Among the presented models the Bouc-Wen model [2] is to be one of the most accurate. The Bouc-Wen model consists of hysteresis component defined using a nonlinear differential equation accompanied with linear viscous damping and stiffness components. Thus, simulation of the Bouc-Wen model requires more complex solvers comparing to static MR damper models. Furthermore, nonlinearity of such model makes its identification complex and not unique. It was also reported that the Bouc-Wen model exhibits greater inaccuracy for modelling force saturation in the postyield [24]. However, the Bouc-Wen model is defined in a compact form which map major features of MR damper behaviour, that is, hysteresis loops, force saturation, and additional viscous damping and stiffness indicated by MR damper behaviour. Furthermore, the hysteresis component can more accurately, in comparison to, for example, Tanh model, map hysteretic behaviour for nonharmonic and wideband piston excitations, apart from sinusoidal excitations. Parameters of the Bouc-Wen obtained for different control currents were additionally approximated using higher-degree polynomial in the presented paper in order to more accurately fit variations of parameters.

According to the Bouc-Wen model, force yield by the MR damper is defined as follows:

$$F_{mr,bw} = -\left[c_{bw} v_{mr} + k_{bw}\left(z_{mr} - x_{bw}\right) + \alpha_{bw} p\right], \quad (3)$$

where v_{mr} denotes relative velocity of MR damper piston and c_{bw}, k_{bw}, α_{bw}, and x_{bw} denote parameters of the model. The hysteretic displacement p is described by the first-order nonlinear differential equation:

$$\dot{p} = -\gamma_{bw} \cdot \left|v_{mr}\right| \cdot p \cdot \left|p\right|^{n-1} - \beta_{bw} v_{mr} \left|p\right|^{n} + A_{bw} v_{mr}, \quad (4)$$

where symbols γ_{bw}, β_{bw}, and A_{bw} denote the additional parameters of the Bouc-Wen model.

Commonly, parameters of the Bouc-Wen model are estimated separately for different levels of the control current denoted as i_{mr}. Since the relationship between the current and the model parameters is strongly nonlinear, it is generally approximated using the higher-order polynomials. It was shown in [28] that two parameters α_{bw} and c_{bw} can be related to the control current using the third-order polynomials as follows:

$$\alpha_{bw} = \sum_{j=0}^{3} \alpha_{j,bw} \cdot i_{mr}^{j},$$
$$c_{bw} = \sum_{j=0}^{3} c_{j,bw} \cdot i_{mr}^{j}. \quad (5)$$

Other parameters can be assumed as constant. Parameters of the Bouc-Wen model (see the list below) were estimated based on the identification results presented in [16].

Parameters of the MR Damper Models

Bouc-Wen Model of the MR Damper

$i_{mr} \in (0.0; 1.33)$ A,
$t_{mr} = 12$ ms,
$n = 2$,
$k_{bw} = 0.001$,
$x_{bw} = 1.5$,
$[\alpha_{0,bw}, \alpha_{1,bw}, \alpha_{2,bw}, \alpha_{3,bw}] = [93506, 888021, 27374, -294583]$,
$[c_{0,bw}, c_{1,bw}, c_{2,bw}, c_{3,bw}] = [792, 4195, -6390, 2565]$,
$\gamma_{bw} = 987288$,
$\beta_{bw} = 983237$,
$A_{bw} = 7.979$.

Tanh Based Model of the MR Damper

$\alpha_{0,th} = -23.05$,
$\alpha_{1,th} = 1215$,
$\beta_{th} = 36.47$,
$\gamma_{th} = 1.6$,
$c_{th} = 1203$,
$k_{th} = 1297$.

Furthermore, it was shown in [29] that the response time of the force yield by the MR damper depends on both the control current level and the kinematic excitation of the damper piston, and it can vary from 20 to 40 ms. Thus, the first-order filter $S_{F_{mr}}$ with a time constant t_{mr} equal to 12 ms was included at the output of the Bouc-Wen model to simulate this delay. Within the simulation environment, the MR damper force F_{mr} is processed using $S_{F_{mr}}$ filter resulting in the modified force denoted as F_{mr}^{*}. In this paper the Bouc-Wen model is treated as a reference model included in the vehicle suspension model (see Figure 4).

3. Control Algorithm

Here, the goal of control is to increase the ride comfort, that is, simultaneous mitigation of the heave and pitch vibrations. Results obtained for mixed Skyhook and FxLMS control will be compared with two other algorithms of the semiactive vibration control, that is, the Skyhook algorithm related to the quarter-car model and the two-dimensional Skyhook control optimized with respect to either heave or pitch. All these algorithms belong to the group of the feedback control; they use several response signals available from the vehicle. Mainly, for vibration control, heave and pitch velocities as well as front and rear body velocities are assumed as error signals. Furthermore, the relative displacement and velocity of the MR damper pistons are required for application of the MR damper inverse model. The MR damper displacement can be commonly measured in the experimental vehicle whereas the velocity needs to be estimated.

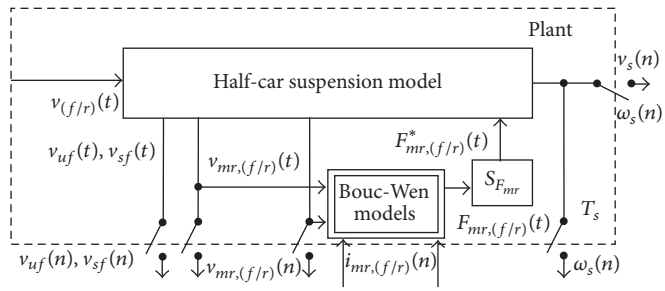

Figure 4: Block diagram of the vehicle simulator.

3.1. Inverse Tanh MR Damper Model. Common semiactive vibration control algorithms require the inverse MR damper model in order to partly linearise nonlinear relationships of the signal path from the input control current to the output MR damper force. Because this model should be used in a control system and solution of the Bouc-Wen inverse model cannot be obtained in the embedded controller in real-time, so for the purpose of vibration control it is proposed to use the hyperbolic tangent function [30] to model nonlinear behaviour of the MR damper as follows:

$$\begin{aligned} &F_{mr,th}\left(i_{mr}, z_{mr}, v_{mr}\right) \\ &\quad = -\left(\alpha_{0,th} + \alpha_{1,th}\sqrt{i_{mr}}\right)\tanh\left[\beta_{th}v_{mr} + \gamma_{th}\,\mathrm{sign}\left(z_{mr}\right)\right] \\ &\qquad - c_{th}v_{mr} - k_{th}z_{mr}, \end{aligned} \tag{6}$$

where symbols $\alpha_{0,th}$, β_{th}, γ_{th}, c_{th}, and k_{th} denote parameters of the model not related to the control current. The parameter $\alpha_{1,th}$ maps the influence of the control current on the MR damper force using a square root operator. Procedure of the *tanh* model identification is presented in [30] and model parameters are listed in Parameters of the MR Damper Models in Section 2.2.

Thus, the inverse model can be easily evaluated from (6) as follows:

$$\begin{aligned} &i_{mr,th} \\ &\quad = \frac{1}{\alpha_{1,th}^2}\left(\frac{-F_{\mathrm{alg}} - c_{th}v_{mr} - k_{th}z_{mr}}{\tanh\left[\beta_{th}v_{mr} + \gamma_{th}\,\mathrm{sign}\left(z_{mr}\right)\right]} - \alpha_{0,th}\right)^2, \end{aligned} \tag{7}$$

where $i_{mr,th}$ stands for the desired control current, which should be generated by the control system in order to make the MR damper generate the desired force F_{alg}.

Additionally, the impact of modelling error on the final result of the damping system was tested. Model identification was repeated for the data contaminated by noise added to force values, and the model thus obtained was used in the control algorithm. It turned out that the results of damping did not differ substantially from the initial inverse model, which may indicate good tolerance to modelling errors.

3.2. Skyhook Control. Control force desired by the Skyhook algorithm related to the quarter-car model is expressed as follows [1]:

$$F_{\mathrm{alg},(f/r)}(n) = -g_{v_{s(f/r)}} \cdot v_{s(f/r)}(n), \tag{8}$$

where $g_{v_{s(f/r)}}$ denotes the gain of Skyhook control for the front or rear part of the vehicle, respectively.

The Skyhook approach can be generalised and extended to the two-dimensional clipped LQ (linear quadratic) control related to the half-car model [5, 31], where the following cost function is minimized:

$$J = \int_0^\infty \left[\mathbf{x}^T(\tau)\,\mathbf{Q}\mathbf{x}(\tau) + \mathbf{F_{alg}}^T(\tau)\,\mathbf{R}\mathbf{F_{alg}}(\tau)\right]d\tau. \tag{9}$$

The diagonal cost matrices $\mathbf{Q}$ and $\mathbf{R}$ related to the vectors $\mathbf{x}$ and $\mathbf{F_{alg}}$ of state and control variables, respectively, are evaluated according to Bryson's rule [32]:

$$\begin{aligned} \mathbf{Q} &= \mathbf{S_x}^{-2}, \\ \mathbf{R} &= \mathbf{S_{F_{alg}}}^{-2}, \end{aligned} \tag{10}$$

where diagonal elements of matrices $\mathbf{S_x}$ and $\mathbf{S_{F_{alg}}}$ are the limitations set on the state- $\mathbf{x}$ and control-related $\mathbf{F_{alg}}$ vectors. Herein, the analysis is focused only on two limitations included in matrix $\mathbf{S_x}$, strictly s_{v_s} and s_{ω_s} related to the v_s and ω_s state variables. The vectors of state and control variables are defined as follows:

$$\begin{aligned} \mathbf{x} &= \left[\left(z_{uf} - z_{rf}\right)\ \ v_{uf}\ \ \left(z_{ur} - z_{rr}\right)\ \ v_{ur}\ \ \left(z_{sf} - z_{uf}\right)\ \ \left(z_{sr} - z_{ur}\right)\ \ v_s\ \ \omega_s\right]^T, \\ \mathbf{F_{alg}} &= \left[F_{\mathrm{alg},f}, F_{\mathrm{alg},r}\right]^T. \end{aligned} \tag{11}$$

The vector $\mathbf{x}$ consists of the vehicle suspension deflections and velocities related to the vehicle body heave and pitch as well as the deflections of tires and absolute velocities of the wheels. In the case of the clipped LQ control forces generated by the MR dampers are assumed as control signals included in the vector $\mathbf{F_{alg}}$.

Reformulation of a set of differential equations (1) and (2) gives the following state matrix equation of the linear half-car model:

$$\dot{\mathbf{x}} = \mathbf{A} \cdot \mathbf{x} + \mathbf{B_F} \cdot \mathbf{F_{alg}} + \mathbf{B_r} \cdot \mathbf{u_r}, \tag{12}$$

where $\mathbf{u_r} = [z_{rf}, v_{rf}, z_{rr}, v_{rr}]^T$ denotes vector of disturbances of the system, that is, road-induced displacement and velocity of the front and rear vehicle part, respectively. Matrices $\mathbf{A}$ and $\mathbf{B_F}$ are expressed as follows:

$$\mathbf{A} = \begin{bmatrix} \mathbf{a_1} & \mathbf{a_2} & \mathbf{a_3} & \mathbf{a_4} & \mathbf{a_5} & \mathbf{a_6} & \mathbf{a_7} & \mathbf{a_8} \end{bmatrix}, \tag{13}$$

where

$$\begin{aligned}
\mathbf{a_1} &= \begin{bmatrix} 0 & -\dfrac{k_{uf}}{m_{uf}} & 0 & 0 & 0 & 0 & 0 & 0 \end{bmatrix}^T, \\
\mathbf{a_2} &= \begin{bmatrix} 1 & \left(-\dfrac{c_{uf}}{m_{uf}} - \dfrac{c_{sf}}{m_{uf}}\right) & 0 & 0 & -1 & 0 & \dfrac{c_{sf}}{m_s} & -\dfrac{L_f c_{sf}}{I_{sL}} \end{bmatrix}^T, \\
\mathbf{a_3} &= \begin{bmatrix} 0 & 0 & 0 & -\dfrac{k_{ur}}{m_{ur}} & 0 & 0 & 0 & 0 \end{bmatrix}^T, \\
\mathbf{a_4} &= \begin{bmatrix} 0 & 0 & 1 & \left(-\dfrac{c_{ur}}{m_{ur}} - \dfrac{c_{sr}}{m_{ur}}\right) & 0 & -1 & \dfrac{c_{sr}}{m_s} & \dfrac{L_r c_{sr}}{I_{sL}} \end{bmatrix}^T, \\
\mathbf{a_5} &= \begin{bmatrix} 0 & \dfrac{k_{sf}}{m_{uf}} & 0 & 0 & 0 & 0 & -\dfrac{k_{sf}}{m_s} & \dfrac{L_f k_{sf}}{I_{sL}} \end{bmatrix}^T, \\
\mathbf{a_6} &= \begin{bmatrix} 0 & 0 & 0 & \dfrac{k_{sr}}{m_{ur}} & 0 & 0 & -\dfrac{k_{sr}}{m_s} & -\dfrac{L_r k_{sr}}{I_{sL}} \end{bmatrix}^T, \\
\mathbf{a_7} &= \begin{bmatrix} 0 & \dfrac{c_{sf}}{m_{uf}} & 0 & \dfrac{c_{sr}}{m_{ur}} & 1 & 1 & \left(-\dfrac{c_{sf}}{m_s} - \dfrac{c_{sr}}{m_s}\right) & \left(\dfrac{L_f c_{sf}}{I_{sL}} - \dfrac{L_r c_{sr}}{I_{sL}}\right) \end{bmatrix}^T, \\
\mathbf{a_8} &= \begin{bmatrix} 0 & -\dfrac{L_f c_{sf}}{m_{uf}} & 0 & \dfrac{L_r c_{sr}}{m_{ur}} & -L_f & L_r & \left(\dfrac{L_f c_{sf}}{m_s} - \dfrac{L_r c_{sr}}{m_s}\right) & \left(-\dfrac{L_f^2 c_{sf}}{I_{sL}} - \dfrac{L_r^2 c_{sr}}{I_{sL}}\right) \end{bmatrix}^T, \\
\mathbf{B_F} &= \begin{bmatrix} \mathbf{b_1} & \mathbf{b_2} \end{bmatrix},
\end{aligned} \tag{14}$$

where

$$\begin{aligned}
\mathbf{b_1} &= \begin{bmatrix} 0 & -\dfrac{\sin(\alpha_{mr,f})}{m_{uf}} & 0 & 0 & 0 & 0 & \dfrac{\sin(\alpha_{mr,f})}{m_s} & -L_f \dfrac{\sin(\alpha_{mr,f})}{I_{sL}} \end{bmatrix}^T, \\
\mathbf{b_2} &= \begin{bmatrix} 0 & 0 & 0 & -\dfrac{\sin(\alpha_{mr,r})}{m_{ur}} & 0 & 0 & \dfrac{\sin(\alpha_{mr,r})}{m_s} & L_r \dfrac{\sin(\alpha_{mr,r})}{I_{sL}} \end{bmatrix}^T.
\end{aligned} \tag{15}$$

They are used for evaluation of the LQ time-infinite problem with the solution of the continuous time algebraic Riccati equation:

$$\mathbf{A}^T\mathbf{P} + \mathbf{P}\mathbf{A} + \mathbf{P}\mathbf{B_F}\mathbf{R}^{-1}\mathbf{B_F}^T\mathbf{P} + \mathbf{Q} = \mathbf{0}. \tag{16}$$

The solution $\mathbf{P}$ of (16) is applied for evaluation of the control gain as follows:

$$\mathbf{G} = \mathbf{R}^{-1}\mathbf{B}^T\mathbf{P}. \tag{17}$$

In order to retain the same experimental conditions for all algorithms, the clipped LQ control was limited to only two measurable state variables, heave and pitch velocities, resulting in the following control force for the front or rear suspension MR damper:

$$F_{\mathrm{alg},(f/r)}(n) = -g_{v_s,(f/r)} \cdot v_s(n) - g_{\omega_s,(f/r)} \cdot \omega_s(n), \tag{18}$$

where gains $g_{v_s,(f/r)}$ and $g_{\omega_s,(f/r)}$ are selected elements of the control gain matrix $\mathbf{G}$ evaluated according to (17).

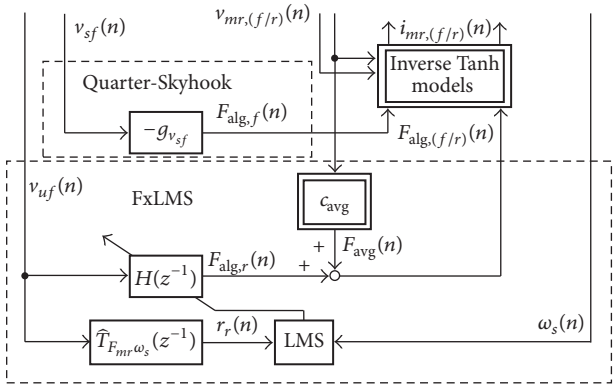

Figure 5: Block diagram of the mixed Skyhook and FxLMS control.

3.3. Mixed Skyhook and FxLMS Control. The FxLMS (Filtered-x LMS) algorithm is an example of adaptive feedforward control commonly applied in active noise control [33]. The idea of using the modified FxLMS algorithm for vibration control in semiactive suspension was introduced in [16]. It was assumed that the experimental vehicle is equipped with an additional device scanning the road profile and the algorithm takes advantage of the reference signal generated by this device. Here, in order to simplify the control system, it is assumed that instead of the reference signal taken from the scanner, we can use a signal obtained from the sensor measuring the motion of the front vehicle axle v_{uf} as the reference signal for the feedforward control of the rear damper. Thus, the front MR damper should be controlled by the classical Skyhook scheme related to the quarter-car model (8), whereas the rear MR damper can be controlled by the modified FxLMS algorithm, which results in a control scheme presented in Figure 5. Here, relative motion of the MR damper pistons and motion of other vehicle parts, particularly the vehicle body and axles, are available at the output of the vehicle dynamics simulator.

Similar to the previously referred Skyhook control, the goal of the adaptive algorithm related to the rear vehicle part is to minimize pitch vibrations of the vehicle body. Parameters of the adaptive FIR (Finite Impulse Response) filter $H(z^{-1})$ are updated according to the following expression:

$$\mathbf{h}(n+1) = \gamma \mathbf{h}(n) - \mu \cdot \omega_s(n) \cdot \frac{\mathbf{r}(n)}{\mathbf{r}^T(n) \cdot \mathbf{r}(n) + \zeta}, \quad (19)$$

where $\mu = 0.007$ is the adaptation step of the algorithm. Leakage of the FxLMS algorithm is controlled by γ equal to 0.997. For semiactive devices with the significant force saturation, the leakage parameter is introduced to ensure stability of the algorithm. Parameter $\zeta = 10^{-15}$ is used to avoid division by zero in the case of zeroing $\mathbf{r}(n)$. The parameters mentioned above were adjusted experimentally.

The reference signal $r(n)$ is obtained by filtering the vertical velocity of the front vehicle axle z_{uf} by the appropriate model of the secondary path $\widehat{T}_{F_{mr}\omega_s}(z^{-1})$. This signal path was estimated starting from the force generated by the rear MR damper and ending with the pitch velocity assuming that the additional viscous damper was added to the vehicle suspension. This fictitious damper equivalent to the averaged velocity-force characteristics is used for modification of the dissipative domain of the MR damper, as it was shown in [16]. Operator z^{-1} presented in Figure 5 corresponds to a one-sample delay. Consecutive M samples of $r(n)$, where $M = 128$ is the selected experimentally length of the filter $H(z^{-1})$, create the vector $\mathbf{r}$.

Control signal $F_{\mathrm{alg},r}(n)$ is generated as a result of filtering v_{uf} using the adaptive filter $H(z^{-1})$. Additionally, F_{avg} generated by the fictitious passive damper c_{avg} according to $v_{mr,r}$ related to the rear part of the vehicle is added to the $F_{\mathrm{alg},r}(n)$. Finally, the desired control current $i_{mr,(f/r)}$ is calculated using the inverse MR damper model (7).

4. Results

Simulation environment consists of two time domains related to the simulation of the vehicle dynamics and to vibration control. The differential equations related to the half-car model (1) and (2) and the Bouc-Wen model (3) and (4) were numerically solved using the Runge-Kutta method with variable integration step and interpolated for the sampling interval $T_{s,\mathrm{model}} = 1$ ms, whereas the control algorithm was executed with the sampling interval $T_{s,\mathrm{control}} = 2$ ms. It reflects the real experimental setup with a digital controller.

In the first stage the analysis was carried out in time domain based on heave and pitch acceleration presented for in-phase and antiphase road-induced excitation, respectively. The first resonant frequency of the analysed half-car model is close to 2 Hz. Thus, time diagrams of heave acceleration are presented for road-induced excitation of such frequency in order to clearly show differences in damping the heave resonant peak for all algorithms (see Figure 6). In the case of pitch acceleration the greatest differences in control performance were found for excitation frequency equal to 4.8 Hz. It can be noticed in time diagrams that 2-dimensional heave or pitch Skyhook exhibits good performance for only one in-phase or antiphase case of excitation. Control quality offered by quarter-Skyhook and mixed Skyhook-FxLMS algorithm is comparable, where the latter one is slightly better in mitigation of pitch vibration.

4.1. Transmissibility Characteristics and Control Quality Assessment. Analysis of vibration control was performed within the frequency range from 1.0 to 10 Hz, as the most of vibration modes of the vehicle dynamics occur within this range. In-phase and antiphase road-induced excitation of the front and rear wheels are critical for the different heave and pitch vibration modes, respectively. Thus, the heave transmissibility characteristics and the related quality index were evaluated for the in-phase excitation of both wheels, whereas the pitch dynamics was analysed for the antiphase excitation, that is, when the peak at the front wheel meets with the valley at the rear wheel, or vice versa. The evaluation procedure for the algorithms was carried out in two stages. Generally, the quality of vibration control is evaluated using

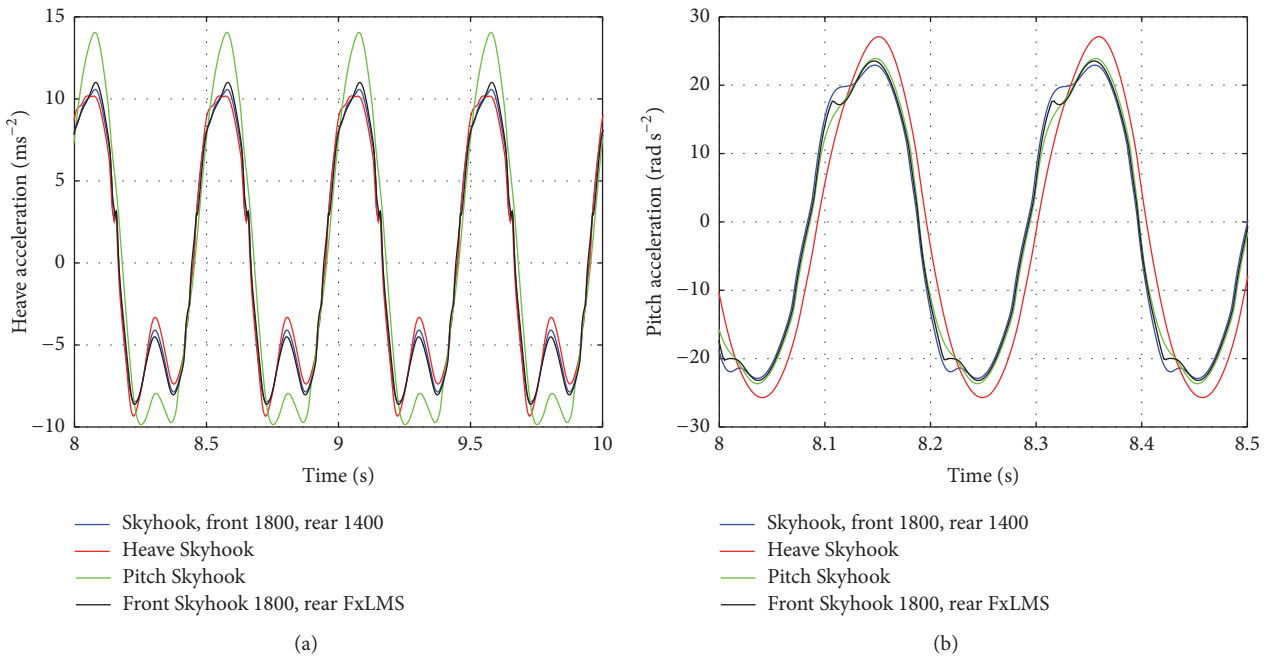

FIGURE 6: Comparison of algorithms in time domain: (a) heave acceleration for in-phase road-induced excitation of 2 Hz and (b) pitch acceleration for antiphase road-induced excitation of 4.8 Hz.

the velocity or acceleration transmissibility characteristics. The velocity transmissibility is defined for the heave v_s as

$$T_{v_r,v_s}(f) = \sqrt{\frac{\sum_{n=1}^{N} v_s^2(n)}{\sum_{n=1}^{N} v_r^2(n)}}\Bigg|_f \tag{20}$$

and for the pitch ω_s as

$$T_{v_r,\omega_s}(f) = \sqrt{\frac{\sum_{n=1}^{N} \omega_s^2(n)}{\sum_{n=1}^{N} v_r^2(n)}}\Bigg|_f. \tag{21}$$

The acceleration transmissibility is defined for the heave a_s as

$$T_{a_r,a_s}(f) = \sqrt{\frac{\sum_{n=1}^{N} a_s^2(n)}{\sum_{n=1}^{N} a_r^2(n)}}\Bigg|_f \tag{22}$$

and for the pitch ε_s as

$$T_{v_r,\varepsilon_s}(f) = \sqrt{\frac{\sum_{n=1}^{N} \varepsilon_s^2(n)}{\sum_{n=1}^{N} a_r^2(n)}}\Bigg|_f. \tag{23}$$

These characteristics are calculated assuming the vehicle is excited with a series of the road bumps with varying frequency f and the velocity amplitude $A = 0.3\,\mathrm{ms}^{-1}$, invariant over the whole frequency range.

Besides, the algorithms were compared using the following normalized quality indices based on the heave velocity transmissibility characteristics:

$$J_{v_s} = \frac{\sum_{1\,\mathrm{Hz}}^{10\,\mathrm{Hz}} T_{v_r,v_s}(f)\,\Delta f}{\sum_{1\,\mathrm{Hz}}^{10\,\mathrm{Hz}} T_{0,v_r,v_s}(f)\,\Delta f} \tag{24}$$

and on the pitch velocity transmissibility characteristics:

$$J_{\omega_s} = \frac{\sum_{1\,\mathrm{Hz}}^{10\,\mathrm{Hz}} T_{v_r,\omega_s}(f)\,\Delta f}{\sum_{1\,\mathrm{Hz}}^{10\,\mathrm{Hz}} T_{0,v_r,\omega_s}(f)\,\Delta f}, \tag{25}$$

where $T_{0,v_r,v_s}(f)$ and $T_{0,v_r,\omega_s}(f)$ denote the reference heave and pitch velocity transmissibility characteristics evaluated for the soft passive suspension, that is, for control currents equal to zero. Furthermore, the following normalized quality indices based on acceleration transmissibility characteristics were also analysed:

$$J_{a_s} = \frac{\sum_{1\,\mathrm{Hz}}^{10\,\mathrm{Hz}} T_{a_r,a_s}(f)\,\Delta f}{\sum_{1\,\mathrm{Hz}}^{10\,\mathrm{Hz}} T_{0,a_r,a_s}(f)\,\Delta f} \tag{26}$$

and on the pitch velocity transmissibility characteristics:

$$J_{\varepsilon_s} = \frac{\sum_{1\,\mathrm{Hz}}^{10\,\mathrm{Hz}} T_{a_r,\varepsilon_s}(f)\,\Delta f}{\sum_{1\,\mathrm{Hz}}^{10\,\mathrm{Hz}} T_{0,a_r,\varepsilon_s}(f)\,\Delta f}. \tag{27}$$

The quality indices are evaluated based on the heave and pitch transmissibilities interpolated with frequency resolution denoted as $\Delta f = 0.1\,\mathrm{Hz}$.

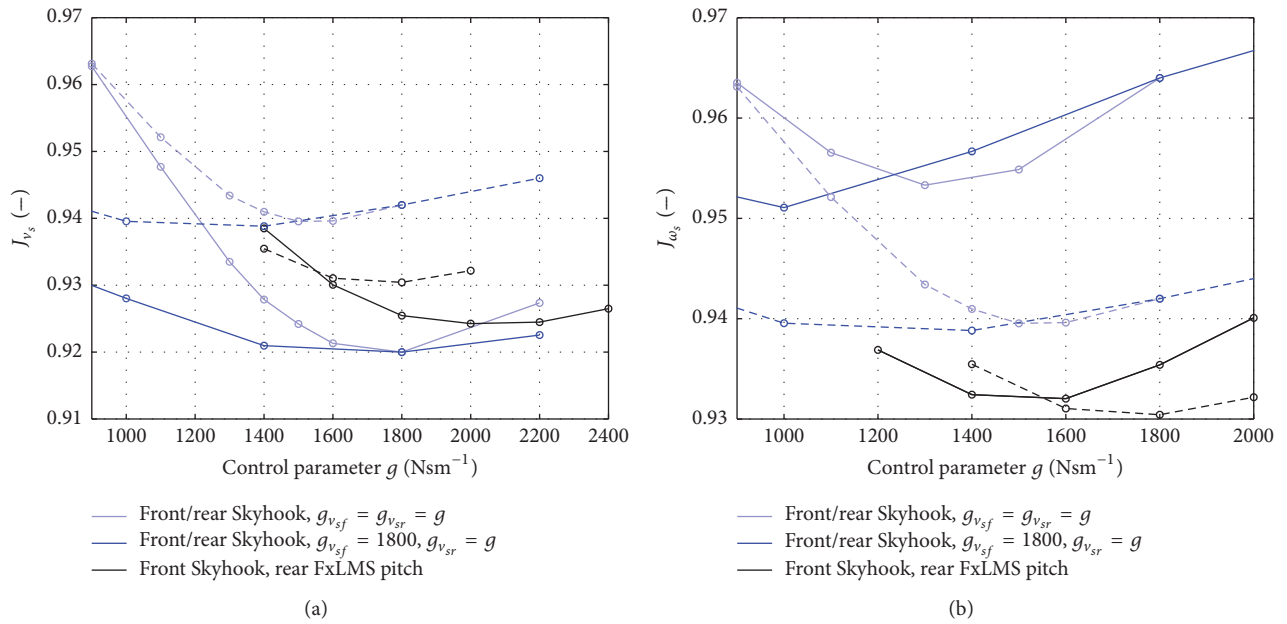

Figure 7: Comparison of vibration control quality for the front/rear Skyhook and mixed Skyhook-FxLMS algorithms: (a) the heave index for the front and rear excitation in phase and (b) the pitch index for the front and rear excitation in antiphase. Dashed lines—the average of J_{v_s} and J_{ω_s}.

4.2. Optimization and Validation of Vibration Control Algorithms. In order to properly indicate advantages of the proposed mixed Skyhook-FxLMS algorithm in comparison to the well-known quarter- and two-dimensional Skyhook control, the latter algorithms need to be initially optimized. The optimization is not a trivial task since the Skyhook control is nonadaptive whereas the vehicle model is highly nonlinear. Thus, the optimal gain in the algorithm was determined by a trial-and-error method, which requires a series of experiments to be performed. The proper value of the gain depends mainly on the suspension parameters. The values corresponding to the damping coefficients presented in Parameters of the Simulated 4 DOFs Half-Car Model in Section 2.1 can be used as a starting point for the search procedure. On the other hand, the gain depends weakly on the amplitude of the excitation or generally on the road class, as it was shown in [34]. However, it was also observed that the choice of the gain is not crucial for the efficiency of vibration mitigation as it varies little over a wide range of gain values (see Figures 7 and 9).

All presented algorithms were compared using vibration control quality indices defined by (24)–(27) and evaluated for the different quarter-Skyhook parameters $g_{v_{s(f/r)}}$ as well as the different two-dimensional Skyhook parameters $g_{v_s(f/r)}$ and $g_{\omega_s(f/r)}$. Herein, results are presented only for the quality indices which are based on velocity quantities. The control parameters were being adjusted for each algorithm in a wide range in order to find an optimized configuration for each of them. An example of a set of heave velocity transmissibility characteristics is presented in Figure 8, where results were obtained for different values of s_{v_s} parameter of heave Skyhook algorithm which was synthesized focusing on

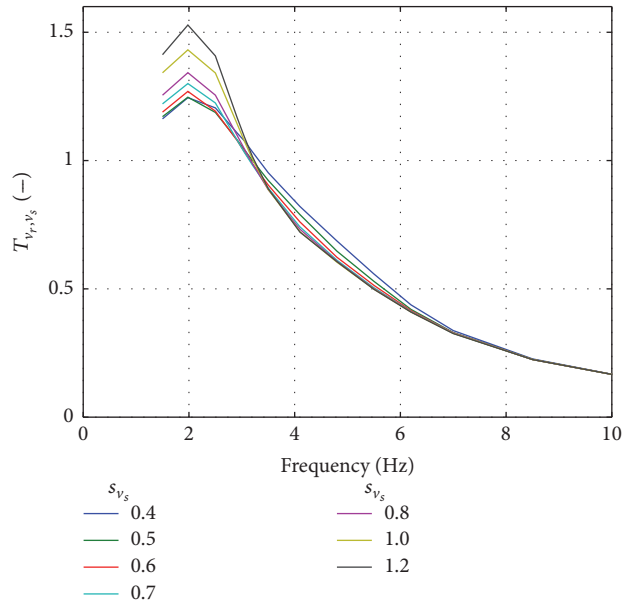

Figure 8: Comparison of heave Skyhook algorithm in frequency domain for different values of control parameters and for in-phase road-induced excitation.

mitigation of heave vibration mode. Thus, changing s_{v_s} can lead to heave Skyhook algorithm which is underactuated, optimized or overactuated particularly for the 2 Hz resonant frequency related to the heave mode.

The quarter-Skyhook was validated in two stages with respect to the averaged quality index. Firstly, control gains were assumed to be the same for the front and rear vehicle

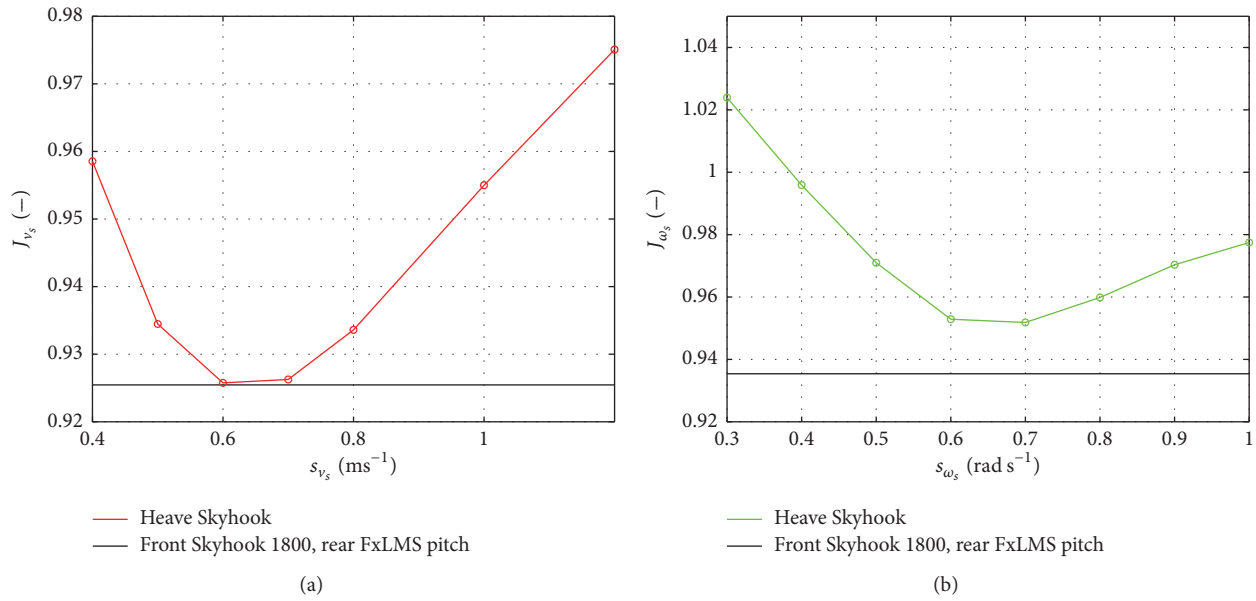

Figure 9: Mixed Skyhook/FxLMS versus 2-dimensional Skyhook optimized with respect to (a) heave mitigation or (b) pitch mitigation.

suspension which gave an optimized control quality for $g_{v_{sf}}$ and $g_{v_{sr}}$ equal to 1800. Secondly, neighbourhood of the solution space of such parameters, changing both of them, was examined which gave improved Skyhook control for $g_{v_{sf}}$ = 1800 and $g_{v_{sr}}$ = 1400.

Figure 7 shows a comparison of the quarter-Skyhook and the mixed Skyhook-FxLMS control approaches. Both cases of Skyhook control parameters were presented, that is, the same values of $g_{v_{sf}}$ and $g_{v_{sr}}$ as well as $g_{v_{sf}}$ equal to 1800 and varying $g_{v_{sr}}$. The characteristics were evaluated for the road-induced excitation of the front and rear vehicle in phase and antiphase. It can be seen that vibration control for both algorithms is comparable for the in-phase excitation; however, the difference is clearly visible for the antiphase excitation. Besides, the averaged value of both quality indices was shown for the Skyhook algorithm which confirms that mixed Skyhook-FxLMS is recommended to be used when both heave and pitch vibrations need to be mitigated.

Next, the two-dimensional heave and pitch Skyhook are treated as a reference algorithm separately for heave and pitch vibrations. Optimization results for both algorithms are presented in Figure 9. The heave and pitch Skyhook were optimized assuming that the weights included in the matrix Q, related to the heave or pitch vibration, respectively, are nonzero. Thus, both the heave or pitch Skyhook are fully focused on mitigation of the selected vehicle vibration modes. It can be noticed that, for the in-phase excitation, the proposed mixed algorithm is slightly better than the Skyhook optimized with respect to the heave, and for the antiphase excitation it is significantly better than the Skyhook optimized with respect to the pitch.

Finally, the heave and pitch velocity and acceleration transmissibilities defined by (20)–(23) obtained for mixed Skyhook/FxLMS and quarter-Skyhook and for two-dimensional Skyhook optimized for either heave or pitch mitigation are presented in Figures 10 and 11. It is easy to notice that optimization of the heave Skyhook leads to deterioration of the pitch mitigation and vice versa. Similar conclusions can be drawn based on either velocity or acceleration transmissibilities. The quarter-Skyhook gives good results for heave vibration; however its efficiency is worse in case of mitigation of pitch vibration. On the contrary, mixed Skyhook-FxLMS performs well for both cases. Moreover, all types of Skyhook control, contrary to FxLMS component, require preliminary optimization, which is not an easy task in the case of real road experiments, as it was shown before.

5. Conclusions

The paper deals with vibration control related to the model of the experimental vehicle equipped with the automotive MR dampers. The analysis is carried out based on the 4-DOFs half-car model, which includes the Bouc-Wen model of the MR dampers. The mixed Skyhook/FxLMS control approach was proposed and compared with quarter-Skyhook and clipped LQ control simplified to the two-dimensional Skyhook algorithm optimized with respect to heave or pitch. Here, the FxLMS algorithm implemented for control of the rear MR damper uses the vertical velocity signal obtained from the front axle as a reference signal.

The quality of vibration control was analysed based on the heave and pitch velocity transmissibility characteristics as well as on the quality indices related to the vibration control of heave and pitch. Initially, all presented types of Skyhook control were numerically optimized to be properly

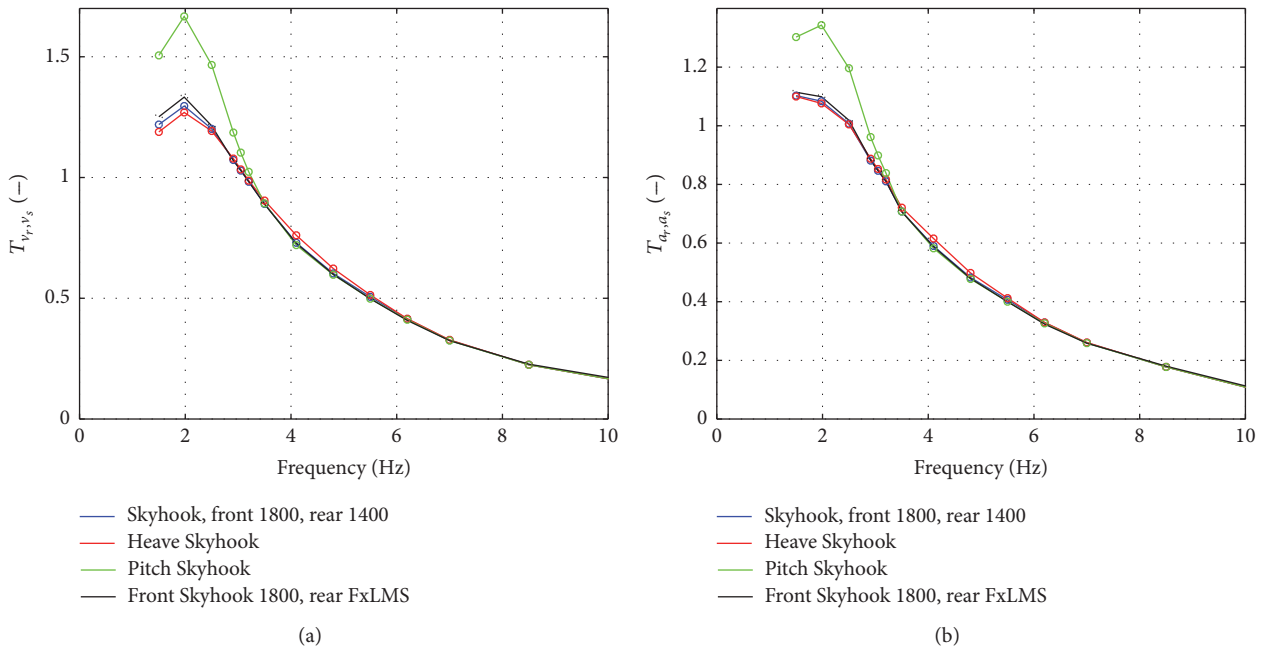

FIGURE 10: Comparison of algorithms in frequency domain for in-phase road-induced excitation based on transmissibilities of (a) heave velocity and (b) heave acceleration.

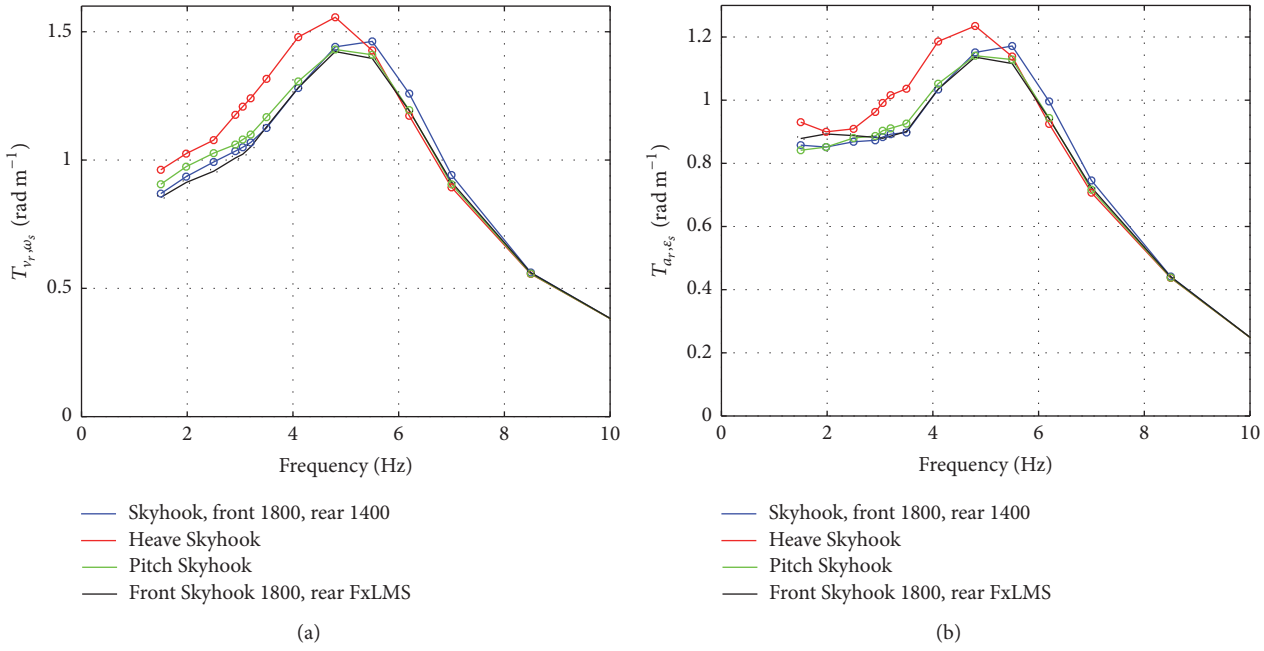

FIGURE 11: Comparison of algorithms in frequency domain for antiphase road-induced excitation based on transmissibilities of (a) pitch velocity and (b) pitch acceleration.

compared with the mixed Skyhook/FxLMS algorithm. Both validation approaches confirmed that the proposed solution should be applied in the case of mitigation of both heave and pitch vibrations. Moreover, this approach is favoured for its adaptability in comparison to the classical Skyhook algorithms.

Competing Interests

The authors confirm that the received funding does not lead to any conflict of interests regarding the publication of this manuscript. Furthermore, the authors declare there is no other possible conflict of interests in the manuscript.

Acknowledgments

The work reported in this paper has been partially financed by the Polish Ministry of Science and Higher Education.

References

[1] D. Karnopp, M. J. Crosby, and R. A. Harwood, "vibration control using semi-active force generators," *Journal of Engineering for Industry, Transactions of ASME*, vol. 96, no. 2, pp. 619–626, 1974.

[2] B. F. Spencer Jr., S. J. Dyke, M. K. Sain, and J. D. Carlson, "Phenomenological model for magnetorheological dampers," *ASCE Journal of Engineering Mechanics*, vol. 123, no. 3, pp. 230–238, 1997.

[3] B. Sapiński, *Magnetorheological Dampers in Vibration Control*, AGH University of Science and Technology Press, Cracow, Poland, 2006.

[4] X. M. Dong, M. Yui, Z. Li, C. Liao, and W. Chen, "A comparison of suitable control methods for full vehicle with four MR dampers, part I: Formulation of control schemes and numerical simulation," *Journal of Intelligent Material Systems and Structures*, vol. 20, no. 7, pp. 771–786, 2009.

[5] P. Krauze, "Comparison of control strategies in a semi-active suspension system of the experimental ATV," *Journal of Low Frequency Noise, Vibration and Active Control*, vol. 32, no. 1-2, pp. 67–80, 2013.

[6] S. Guo, S. Li, and S. Yang, "Improvement of measurement results based on scattered data in cases where averaging is ineffective," in *Proceedings of the IEEE International Conference on Vehicular Electronics and Safety (ICVES '06)*, vol. 13, no. 10, pp. 403–406, Beijing, China, December 2006.

[7] I. Maciejewski, "Modelling and control of semi-active seat suspension with magnetorheological damper," in *Proceedings of the 24th Symposium on Vibrations in Physical Systems*, vol. 13, no. 10, pp. 1–6, Poznan-Bedlewo, Poland, May 2010.

[8] K. Plaza, *Modelling and control for semi-active vibration damping [Ph.D. dissertation]*, Silesian University of Technology, Gliwice, Poland, 2008.

[9] B. Sapiński, *Real-Time Control of Magnetorheological Dampers in Mechanical Systems*, AGH University of Science and Technology Press, Cracow, Poland, 2008.

[10] J.-P. Hyvarinen, *The improvement of full vehicle semi-active suspension through kinematical model [Ph.D. thesis]*, University of Oulu, Oulu, Finnland, 2004.

[11] Y. Cho, B. S. Song, and K. Yi, "Improvement of measurement results based on scattered data in cases where averaging is ineffective," *KSME International Journal*, vol. 13, no. 10, pp. 667–676, 1999.

[12] A. Hać and I. Youn, "Optimal semi-active suspension with preview based on a quarter car model," *Journal of Vibration and Acoustics*, vol. 114, no. 1, pp. 84–92, 1992.

[13] A. Hać and I. Youn, "Optimal design of active and semi-active suspensions including time delays and preview," *Journal of Vibration and Acoustics*, vol. 115, no. 4, pp. 498–508, 1993.

[14] J. Marzbanrad, G. Ahmadi, H. Zohoor, and Y. Hojjat, "Stochastic optimal preview control of a vehicle suspension," *Journal of Sound and Vibration*, vol. 275, no. 3–5, pp. 973–990, 2004.

[15] R. S. Prabakar, C. Sujatha, and S. Narayanan, "Optimal semi-active preview control response of a half car vehicle model with magnetorheological damper," *Journal of Sound and Vibration*, vol. 326, no. 3–5, pp. 400–420, 2009.

[16] P. Krauze and J. Kasprzyk, "Vibration control in quarter-car model with magnetorheological dampers using FxLMS algorithm with preview," in *Proceedings of the 13th European Control Conference (ECC '14)*, pp. 1005–1010, Strasbourg, France, June 2014.

[17] P. Krauze and J. Kasprzyk, "FxLMS algorithm with preview for vibration control of a half-car model with magnetorheological dampers," in *Proceedings of the IEEE/ASME International Conference on Advanced Intelligent Mechatronics (AIM '14)*, pp. 518–523, Besancon, France, July 2014.

[18] S. Budzan and J. Kasprzyk, "Fusion of 3D laser scanner and depth images for obstacle recognition in mobile applications," *Optics and Lasers in Engineering*, vol. 77, pp. 230–240, 2016.

[19] J. Wiora, "Improvement of measurement results based on scattered data in cases where averaging is ineffective," *Sensors and Actuators, B: Chemical*, vol. 201, pp. 475–481, 2014.

[20] H. A. Asl and G. Rideout, "Using lead vehicle response to generate preview functions for active suspension of convoy vehicles," in *Proceedings of the American Control Conference (ACC '10)*, vol. 8671 of *Lecture Notes in Computer Science*, pp. 4594–4600, Baltimore, Md, USA, July 2010.

[21] P. Krauze and J. Kasprzyk, "Vibration control for an experimental off-road vehicle using magnetorheological dampers," in *Proceedings of the International Conference Vibroengineering*, pp. 306–312, Katowice, Poland, October 2014.

[22] D. Hrovat, "Survey of advanced suspension developments and related optimal control applications," *Automatica*, vol. 33, no. 10, pp. 1781–1817, 1997.

[23] X. Song, M. Ahmadian, and S. C. Southward, "Modeling magnetorheological dampers with application of nonparametric approach," *Journal of Intelligent Material Systems and Structures*, vol. 16, no. 5, pp. 421–432, 2005.

[24] X. Q. Ma, S. Rakheja, and C.-Y. Su, "Development and relative assessments of models for characterizing the current dependent hysteresis properties of magnetorheological fluid dampers," *Journal of Intelligent Material Systems and Structures*, vol. 18, no. 5, pp. 487–502, 2007.

[25] B. Sapiński, "Parametric identification of mr linear automotive size damper," *Journal of Theoretical and Applied Mechanics*, vol. 40, no. 3, pp. 703–722, 2002.

[26] E. R. Wang, X. Q. Ma, S. Rakhela, and C. Y. Su, "Modelling the hysteretic characteristics of a magnetorheological fluid damper," *Proceedings of the Institution of Mechanical Engineers, Part D: Journal of Automobile Engineering*, vol. 217, no. 7, pp. 537–550, 2003.

[27] E. R. Wang, X. Q. Ma, S. Rakheja, and C. Y. Su, "Force tracking control of vehicle vibration with mr-dampers," in *Proceedings of the 2005 IEEE International Symposium on Intelligent Control*, pp. 995–1000, Limassol, Cyprus, June 2005.

[28] G. Yang, B. F. Spencer Jr., J. D. Carlson, and M. K. Sain, "Large-scale MR fluid dampers: modeling and dynamic performance considerations," *Engineering Structures*, vol. 24, no. 3, pp. 309–323, 2002.

[29] J.-H. Koo, F. D. Goncalves, and M. Ahmadian, "A comprehensive analysis of the response time of MR dampers," *Smart Materials and Structures*, vol. 15, no. 2, pp. 351–358, 2006.

[30] J. Kasprzyk, J. Wyrwał, and P. Krauze, "Automotive MR damper modeling for semi-active vibration control," in *Proceedings of the IEEE/ASME International Conference on Advanced Intelligent Mechatronics (AIM '14)*, pp. 500–505, Besancon, France, July 2014.

[31] M. Sibielak, W. Rączka, and J. Konieczny, "Modified clipped-LQR method for semi-active vibration reduction systems with hysteresis," *Journal of Solid State Phenomena*, vol. 177, pp. 10–22, 2011.

[32] A. E. J. Bryson and Y.-C. Ho, *Applied Optimal Control: Optimization, Estimation and Control*, Hemisphere Publishing Corporation, 1975.

[33] S. M. Kuo and D. R. Morgan, *Active Noise Control Systems: Algorithms and DSP Implementations*, Wiley Series in Telecommunication and Signal Processing, Wiley-Interscience, 1996.

[34] P. Krauze, *Control of semiactive vehicle suspension system using magnetorheological dampers [Ph.D. dissertation]*, Silesian University of Technology, Gliwice, Poland, 2015.